Macromolecular Chemistry and Physics
www.mcp-journal.de

Layer-by-Layer Formation of Polyamine-Salt Aggregate/Polyelectrolyte Multilayers. Loading and Controlled Release of Probe Molecules from Self-Assembled Supramolecular Networks

*Santiago E. Herrera, Maximiliano L. Agazzi, M. Lorena Cortez, Waldemar A. Marmisollé, Catalina von Bilderling, and Omar Azzaroni**

The use of soft materials as building blocks in layer-by-layer (LbL) assemblies represent a very appealing and useful approach to enhance the loading capacity of thin films. Here, the capacity of positively charged polyamine-salt aggregates (PSAs) based on ionically crosslinked poly(allylamine hydrochloride) (PAH) with phosphate anions (Pi) is explored to act as building blocks in construction of multilayers by alternated deposition with poly(sodium 4-styrenesulfonate). Hybrid thin films are successfully prepared by the LbL technique with a highly regular growth and a material deposition rate higher than the traditional full polyelectrolyte LbL. The loading of bromophenol blue (BPB) is evaluated by integration into PSAs followed by LbL deposition and monitored with UV–vis spectroscopy. Finally, the release of the dye molecules is carried out by exposing the film to different aqueous solutions. It is shown that a fully controlled release can be achieved by simply varying the media pH obtaining total BPB release over periods between minutes and months. The data obtained reveal that this new LbL construction strategy using ionically crosslinked PAH/Pi colloids allows to obtain nanoarchitectures with high loading capacity and remarkable properties for controlled release.

1. Introduction

The development of new functional materials based on thin films with precisely controllable composition and properties has become an exciting challenge in the field of material sciences over the last decade. Within this context, the layer-by-layer (LbL) technique has emerged as a highly powerful approach for the tunable construction of multilayered interfacial architectures that allows incorporating and integrating a broad spectrum of functionalities into the films.[1–4] Initially, LbL technique was explored to create surface coatings from sequential deposition of opposite charge polyelectrolytes.[5] Thereafter, the design of LbL films was significantly expanded toward the supramolecular self-assembly of other charged building blocks such as biomacromolecules, nanoparticles, dendrimers, and lipids.[6–11] The flexibility and versatility of the method allowed generating different materials tailored to multiple applications in areas such as biosensors, electrochemical and optical devices, filtration membranes, biologically active coatings, drug delivery, etc.[12–19]

In many applications, such as controlled release of drugs, it is desirable that the films present matrices with high loading capacity of guest functional materials. Although LbL assembly of polyelectrolytes have been studied for encapsulation and subsequent release of molecules,[20,21] different efforts have been made to generate architectures that present higher loading capacities. In this regard, hydrogels were generated from the covalent and selective crosslinking of a polyelectrolyte in an LbL assembly and subsequent removal of the other non-crosslinked polymer by a specific trigger as the basic pH.[22,23] Zhang and Sun reported on the preparation of coatings with high loading capacity by the LbL deposition of two polyelectrolyte complexes and photo-crosslinked with diazoresin.[24] On the other hand, the use of "soft" nanocapsules as building blocks has become a promising strategy to increase the loading of host molecules in LbL thin films. For instance, matrices with high encapsulation efficiency have been prepared using vesicles or micelles.[25–28] Within this framework, films containing microgel components have aroused interest for their loading capacities and ability to act as responsive materials to various external

Dr. S. E. Herrera, Dr. M. L. Agazzi, Dr. M. L. Cortez, Dr. W. A. Marmisollé, Dr. C. von Bilderling, Prof. O. Azzaroni
Instituto de Investigaciones Fisicoquímicas Teóricas y Aplicadas
Departamento de Química
Facultad de Ciencias Exactas
Universidad Nacional de La Plata–CONICET
Sucursal 4, Casilla de Correo 16, 1900 La Plata, Argentina
E-mail: azzaroni@inifta.unlp.edu.ar
Dr. C. von Bilderling
Departamento de Física
Facultad de Ciencias Exactas y Naturales
Universidad de Buenos Aires
C1428EHA Buenos Aires, Argentina
The ORCID identification number(s) for the author(s) of this article can be found under https://doi.org/10.1002/macp.201900094.

DOI: 10.1002/macp.201900094

stimuli. Lyon and coworkers were the first to report the use of microgels as building blocks in LbL films. They prepared thin films by LbL deposition of thermo-responsive poly(*N*-isopropylacrylamide-co-acrylic acid) microgels with the weak polycation poly(allylamine hydrochloride) (PAH).[29] From those works, the exploration of LbL architectures based on soft materials has considerably increased.[30–35] Sun and collaborators reported films generated by LbL assembly of poly(sodium 4-styrenesulfonate) (PSS) and microgels formed by PAH chains covalently cross-linked with useful loading properties.[36]

More recently, supramolecular colloids based on ionically cross-linked polyelectrolytes have attracted great interest among practitioners from the materials science community due to the simplicity of their preparation and the capacity to integrate different molecules in their matrix.[37] In this regard, bioinspired complexes of ionically cross-linked polyamines with multivalent anions can be formed by a one-step process from the mixture of the precursors in aqueous solution.[38–41] In particular, it was demonstrated that PAH chains spontaneously self-assemble by cross-linking with simple phosphate anions (Pi) to form polyamine-salt aggregates (PSAs) of variable size.[42–46] Yu et al. reported that PSAs can efficiently encapsulate indocyanine green, a fluorescent probe.[47] Very recently, Moya and coworkers observed that these colloids can act as pH-responsive nanocarriers of RNA.[48]

In this context, electrostatically charged PSAs may result in versatile building blocks to create LbL assemblies exhibiting high loading capabilities. Therefore, in the present work we explore the possibility of generating thin films by sequentially assembling PAH/Pi positively charged PSAs with PSS as negative polyelectrolyte. The growth of the hybrid LbL films was compared with that corresponding to the conventional LbL assembly of PAH/PSS in the same experimental conditions. In addition, the loading efficiency of this hybrid platform was evaluated with UV–vis absorption spectroscopy by the encapsulation of an anionic dye probe in each cycle of PSA deposition. Finally, the release of the dye as a function of time in PBS at different pH values was monitored. The results obtained indicate that the use of supramolecular PSAs as building blocks in LbL assembly allows obtaining thin films with attractive properties for the loading of functional materials and their controlled release.

2. Experimental Section

2.1. Chemicals

PAH (Average $M_w \approx 17\,500$), phosphate buffered saline (PBS), PSS (Average $M_w \approx 1\,000\,000$), bromophenol blue (BPB), 3-mercapto-1-propanesulfonic acid sodium salt (MPS), poly(diallyldimethylammonium chloride) solution (PDDA) and potassium chloride were purchased from Sigma-Aldrich. Sodium hydroxide and hydrochloric acid were purchased from Anedra. Sodium phosphate monobasic monohydrate (Pi) was purchased from Cicarelli. All chemicals were used without further purification.

2.2. PSA Colloidal Dispersion Preparation

For the PSAs formation, 25 mL of 2.244 mg mL^{-1} (24 mM in monomer) PAH solution adjusted to pH = 8 was added to 25 mL of 8 mM Pi solution adjusted to pH = 8 in a 100 mL beaker. The resulted colloidal dispersion was kept at room temperature for 24 h to allow stabilization. After this period, the registered pH was 9.25. In order to maximize the long-term stability and avoid slow precipitation, the pH of the solution was re-adjusted from pH = 9.25 to pH = 8.00 with HCl 0.2 M and stored for 1 month prior using.

2.3. Dynamic Light Scattering (DLS) and Zeta Potential

DLS and Zeta potential measurements were carried out with a ZetaSizer Nano (ZEN3600, Malvern, UK) at 20 °C using DTS0012 and DTS1060 disposable cuvettes, respectively. For particle size measurements, 173° backscatter angle configuration with 10 runs (20 s per run) was used for each sample. Particle Zeta potential was determined from the electrophoretic mobility by Laser Doppler Velocimetry using a general-purpose analysis method with 100 runs for each sample.

2.4. Layer by Layer Assembly

LbL assembly was carried out employing the PSA solution as positive building block and PSS as the negative counterpart. UV-Ozone cleaned glass slides were used as substrates for AFM and UV–vis experiments. MPS modified Au substrates were used for SPR experiments. Prior to each PSA/PSS LbL deposition, the substrate was modified with 3-bilayers of PDDA/PSS using 1 mg mL^{-1} PDDA and 1 mg mL^{-1} PSS aqueous solutions containing 0.1 M of KCl in order to create a highly reactive interface for the PSAs deposition. The immersion time for each layer was 5 min.

Then, the PSA/PSS LbL deposition was performed as follows. Firstly, the modified substrate was placed vertically in a small glass container filled with the PSA colloidal dispersion. After 20 min, the substrate was removed and rinsed with copious amount of Milli-Q water. Following a typical LbL procedure, the substrate was then placed in the PSS solution for 10 min and rinsed with Milli-Q water to get a *one*-bilayer $(PSA/PSS)_1$ modified substrate. This cycle was repeated the desired number of times to get a *n*-bilayer-modified substrate, $(PSA/PSS)_n$.

2.5. Surface Plasmon Resonance (SPR) Spectroscopy

SPR detection was carried out using an SPR-Navi 210A (BioNavis Ltd.). SPR gold sensors were used as substrates cleaned by immersion in boiling NH_4OH (28%)/H_2O_2 (100 vol) 1:1 for 15 min. After rinsing with water and ethanol they were modified with MPS to create a negatively charged surface. For this, the gold slides were incubated for 24 h in a 10 mM MPS solution in 10 mM H_2SO_4 and cleaned with water. An

electrochemistry flow cell (SPR321-EC, BioNavis Ltd.) was employed for all measurements. The injection of the solutions (PDDA, PSS, and PSA) was performed manually and SPR angular scans (two wavelength mode) were recorded with no flow in the cell. The temperature was kept at 20 °C. All SPR experiments were processed using the BioNavis Data Viewer software.

2.6. Atomic Force Microscopy (AFM)

Topography of PSA/PSS and PAH/PSS modified glass substrates was analyzed by AFM using a Keysight 9500 AFM in tapping mode. Measurements were performed at 20 °C in air employing a triangular Si cantilever (Olympus AC160TS-R3, f = 347 kHz, K = 26 N m^{-1}). For thickness measurements, the substrates were gently scratched with a soft pin to produce partial removal of the film. Images were processed with Gwyddion 2.52 software to remove the background slope and perform cross-section analysis.

2.7. Loading and Release of BPB in LbL Assembly

Bromophenol blue (BPB) was used as target dye molecule. The loading of BPB into the system was performed by adding 500 µL of a 4 mM BPB aqueous solution into the PSA solution (40 µM final concentration). The blue colored colloidal dispersion obtained (PSA^{BPB}) was used as positive building block for LbL formation employing the same procedure described above. The film growth was monitored with UV–vis spectroscopy by drying the $(PSA^{BPB}/PSS)_n$-modified glass substrates under a stream of nitrogen and recording a UV–vis spectrum between 400 and 800 nm using an opened plastic cuvette. To discard scattering effects, a correction of each spectrum was performed by first subtracting the clean glass spectrum and then subtracting the spectrum baseline.

The release of BPB from the $(PSA^{BPB}/PSS)_{10}$ film was monitored by UV–vis spectroscopy. For this, a 2.5 cm × 1 cm modified glass slide was placed in a closed small glass container filled with 2.5 mL of releasing solution (water, PBS, PBS at pH = 2, 5, 8, and 10.5) for a given period of time. This time was varied according the release kinetics at each condition. Then, an aliquot of 2 mL was extracted and placed in a UV–vis plastic cuvette. Considering that the BPB spectrum is pH dependent, 500 µL of NaOH 2 M was added to the cuvette to be sure that all BPB is in the BPB^{2-} form.[49] A UV–vis spectrum was then recorded between 400 and 800 nm, and the BPB concentration was calculated using a calibration curve of BPB at pH = 13 (Figure S2, Supporting Information). Finally, the net BPB moles released from the film was calculated by applying a dilution factor of 3.9738×10^{-9}. After each measurement, the procedure was repeated using fresh releasing solution until all BPB molecules were released (no peak detection in UV–vis spectrum).

UV–vis experiments were carried out using a Perkin Elmer Lambda 35 spectrometer. All BPB spectrums were measured between 400 and 800 nm using either closed plastic 1 cm path length cuvettes (BPB in solution) or opened plastic cuvettes (BPB film in glass).

3. Results and Discussion

3.1. PSA Preparation

A colloidal dispersion of cross-linked PAH with Pi was obtained by direct mixing of PAH (pH = 8) and Pi (pH = 8). As we previously described, the formation of PSAs is mainly driven by the strong electrostatic interaction between PAH chains and HPO_4^{2-} anions.[50] Depending on the initial state of charge of each reagent, the mixing process can produce changes in the solution pH. This effect was previously studied by Lawrence and Lapitzky for the case of PAH/tripolyphosphate macroscopic complexes, showing that this change arises from the pKa shifting of the species toward high valence states and the consequently proton release or uptake from the solution.[51] In the case of PAH/Pi, if the initial pH is fixed below 7.2, the interaction between PAH and HPO_4^{2-} promotes the deprotonation of $H_2PO_4^-$ anions, thus lowering the pH of the solution. If the initial pH is between 7.2 and 10.2, a net increase in the pH is observed due to the protonation of PAH amine groups, promoted by the PSA formation. When the initial pH is above 10.2, the deprotonation of the polyamine produces the total dissolution of the PSAs by shutting down the electrostatic forces responsible for maintaining the stability of the structure.[50] If the initial pH is fixed at 8, as in this work, a maximum positive shift of 1.25 units is given, indicating total reaction between reagents.

After 24 h of stabilization, the pH reached a stable value of pH = 9.25 and a cloudy colloidal dispersion was observed. DLS measurements showed a distribution of sizes centered at 180 nm with a zeta potential of +25 mV. As the main objective of the present work is to use the ionically cross-linked PAH/Pi colloids as LbL building blocks, the PSAs must: 1) exhibit high zeta potential values to produce an effective charge inversion on the surface;[52] and 2) remain stable in solution during large periods of time, avoiding slow precipitation and possible unspecific deposition over the substrate. To fulfill these requirements, the pH of the PAH/Pi solution was lowered to 8.00 as a post-stabilization treatment. By decreasing the pH, the free amine groups in the PSAs get partially protonated, increasing the zeta potential to +32 mV and consequently, increasing the long-term stability.

The prepared PSA solution was monitored with DLS during a month to evaluate possible changes in size and zeta potential over time. **Figure 1** shows the sample size distribution of the PSA suspension, 2 h (blue line) and 30 days (orange line) after the post-stabilization treatment. A narrow single peak was always observed during the evaluated period demonstrating that the sample consists of a stable homogeneous distribution of particle sizes. During this time, the pH of the solution decreased from 8 to a stable value of 7.3. The polydispersity index remained stable and close to 0.15 indicating that the particles does not tend to form aggregates. The particle zeta potential was also stable at +32 ± 2 mV over the entire evaluated

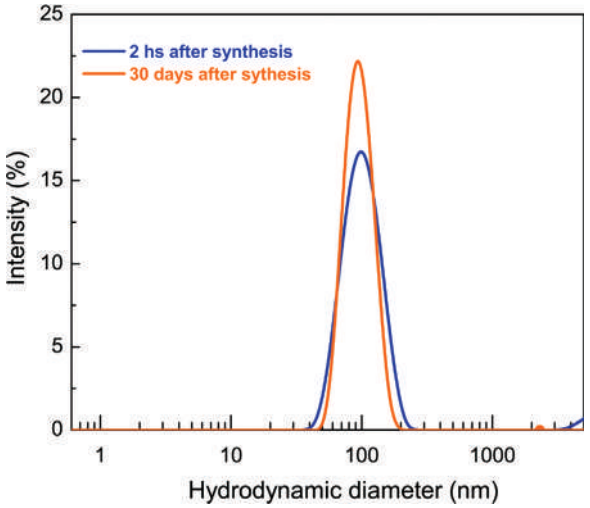

Figure 1. PSAs size distribution at 2 h (blue line) and 30 days (orange line) after synthesis.

period and the count rate obtained from DLS measurements also remained stable at $2.1 \pm 0.2 \times 10^5$ kcps.

3.2. Construction of PSA/PSS Hybrid Multilayer Films

In order to prove the hypothesis that ionically cross-linked PAH/Pi colloids (PSAs) can be deposited over a negatively charged surface in a LbL fashion, SPR spectroscopy characterization was conducted on an Au substrate. To this end, a multilayer film was fabricated by alternated deposition of PSAs and PSS (aqueous solution) as the negatively charged polyelectrolyte (**Scheme 1**). As a comparison, a PAH/PSS film was constructed using the same experimental conditions.

Figure 2a shows the evolution of the angle of minimum reflectivity of gold-coated SPR sensors during the assembly

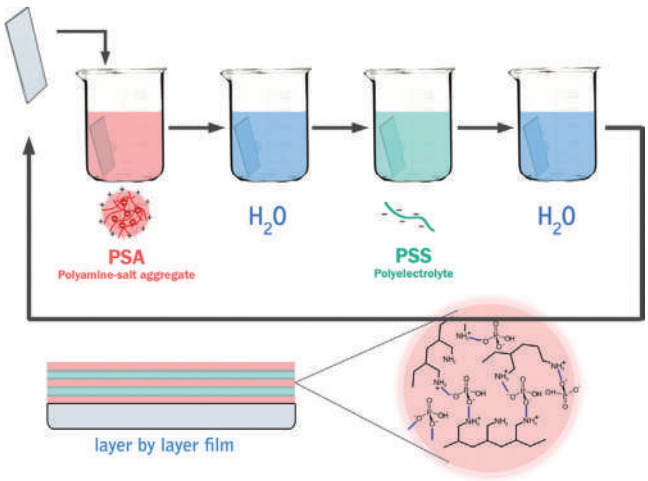

Scheme 1. Layer by layer PSA/PSS film deposition. An alternated deposition loop is carried out obtaining a hybrid film composed by PSS (green film) and a supramolecular network (pink film) of cross-linked PAH chains with phosphate ions.

of the PSA/PSS (orange line) and PAH/PSS (blue line) multilayers. The first six layers correspond to the construction of the $(PDDA/PSS)_3$ surface pre-treatment. The sensograms confirm that PSA supramolecular colloids effectively act as building blocks for LbL deposition, supporting the assembly mechanism proposed in Scheme 1. Also, the growth kinetics of the hybrid film exhibits larger angular shifts per layer than the corresponding traditional full-polyelectrolyte LbL. This implies that the amount of material deposited per assembly cycle is higher than that observed in traditional LbL assembly based on lineal polyelectrolytes. On the other hand, it can be observed that the deposited material remains stable after each rinse cycle, indicating that the assembly is stabilized by specific electrostatic interactions between the PAH/Pi networks and the PSS polymer. Additionally, Figure 2b shows that the change of the minimum reflectivity angle as a function of the number of assembly steps presents a linear behavior starting from the second layer of PSA, thus showing that the PSA/PSS films display a highly regular growth. From this linear film growth, we can infer that the amount of deposited material can be easily modulated by simple variation of the number of assembly steps. Also, the

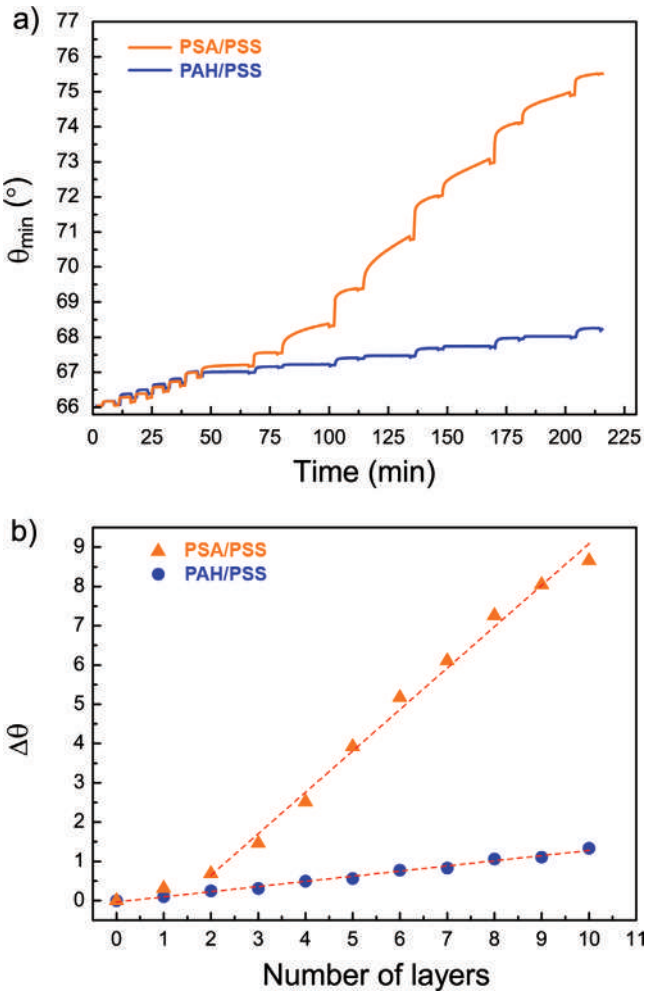

Figure 2. SPR measurements of $(PSA/PSS)_6PSA$ (orange line) and $(PAH/PSS)_6PAH$ multilayer formation. a) Sensograms and b) angle of minimum reflectivity shift ($\Delta\theta$) versus layer number.

regular step-by-step angle variation indicates that both PSA and PSS are more efficiently deposited in comparison with PAH/PSS film. Finally, by conducting a linear regression of each plot (red dotted curves in Figure 2) and comparing the slopes, we found that the growth rate of hybrid PSA/PSS films is eight times higher than the equivalent PAH/PSS film.

Films composed of $(PSA/PSS)_{10}$ were characterized by AFM and compared with the analogous $(PAH/PSS)_{10}$. For these characterizations, glass substrates were coated with PSA/PSS and PAH/PSS multilayers. AFM images obtained for both LbL assemblies are shown in **Figure 3**. $(PSA\ /PSS)_{10}$ films exhibit similar topographic characteristics to the $(PAH/PSS)_{10}$ assembly, showing a fairly homogeneous coating with protuberances of about 60 to 80 nm for $(PAH/PSS)_{10}$ and 250 to 300 nm for $(PSA/PSS)_{10}$. If we consider that the average PAH/Pi particle size is about 100 nm, a homogeneous distribution of material over the surface indicates, in principle, that when the PSA colloids interact with PSS, they tend to integrate into the film without preserving its volume but collapsing in a 2D configuration. This process of structural deformation is quite usual when soft particles are adsorbed at interfaces.[53] During the adsorption, the soft particles can expand in a direction parallel to the surface and compress perpendicularly, losing the 3D conformation and depositing in a pancake-like arrangement.[54–57]

To gain further information of the system, the as-prepared surface was gently scratched with a soft pin to produce a partial removing of the film. On the next, the scratched modified substrate was investigated with AFM searching for the interface between the exposed glass and the multilayer film. The height-profiles taken from the AFM images at the interface showed a thickness value of 80 and 17 nm for $(PSA/PSS)_{10}$ and $(PAH/PSS)_{10}$, respectively. Differences in thickness values for $(PSA/PSS)_{10}$ and $(PAH/PSS)_{10}$ films are in agreement with the higher growth rate observed by SPR measurements for the platforms based on PSA colloids. Also, a value of 80 nm in thickness for ten layers of PAH/Pi prove that the PSAs integrate into the film without preserving the size and shape that they display in solution. This behavior resembles the typical integration of viscoelastic coacervates into surface thin films.[58]

3.3. Loading Efficiency of Films

The integration of a target dye molecule into the hybrid LbL film was studied in order to evaluate the loading efficiency of the new nanoarchitecture. In previous works, microgels based on PAH chains covalently cross-linked with dextran showed appealing properties to optimize the loading of different compounds in LbL films and releasing analytes in a controlled manner.[59–61] However, the synthesis and purification of these microgels require a multi-step process. The possibility of using supramolecular networks generated by the simple mixing in aqueous solution of the polymer and cross-linker significantly reduces the complexity of the building block formation process. In addition, the use of an all-supramolecular approach allows creating platforms with more suitable properties to act as a pH-responsive material.

According to previous studies, the PSAs exhibit a highly permeable structure and can act as host/preconcentrating matrix for small molecules.[39,46–48] In this work, BPB, a negatively charged model dye molecule was selected for the loading tests. As is well-known, BPB presents an acid/base equilibrium with a pKa = 4.[62] Then, if the pH is higher than 7, the BPB molecule (**Figure 4**a) possess a conjugated structure with two negative charges stemming from the changes in the sulfonate moiety and the deprotonation of one of the hydroxyl groups. At alkaline pH (>7) the molecule has a strong absorption band with a maximum at λ = 591 nm and the aqueous solution is blue/purple colored.[49] Considering that PSAs exhibits a positive zeta potential of ≈32 mV, the BPB loading was carried out by adding a small amount of BPB into the pre-formed PSA solution to get a final concentration of 40 μM of BPB. As

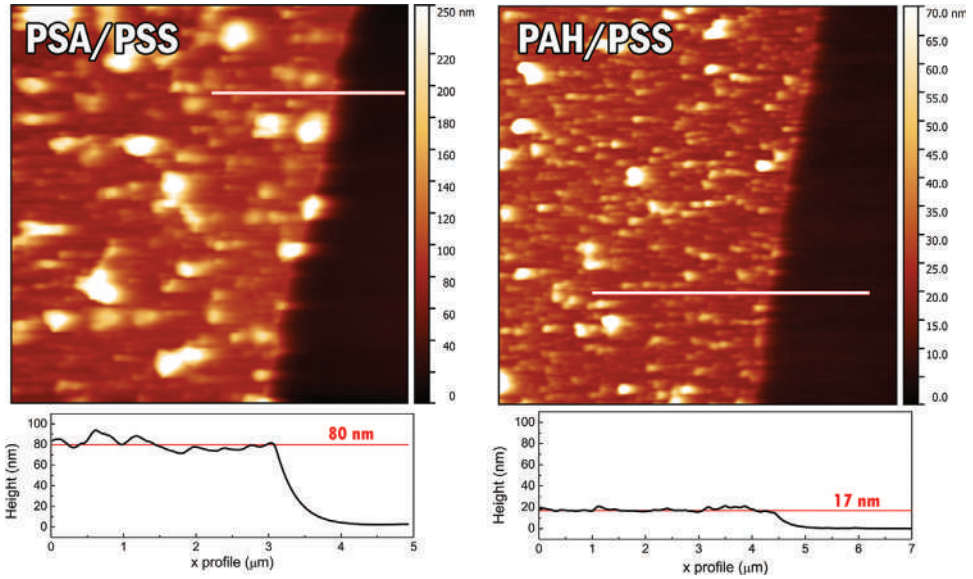

Figure 3. 10 μm × 10 μm AFM topography images of a) $(PAH/PSS)_{10}$, b) $(PSA/PSS)_{10}$ and their respective height profiles in x direction.

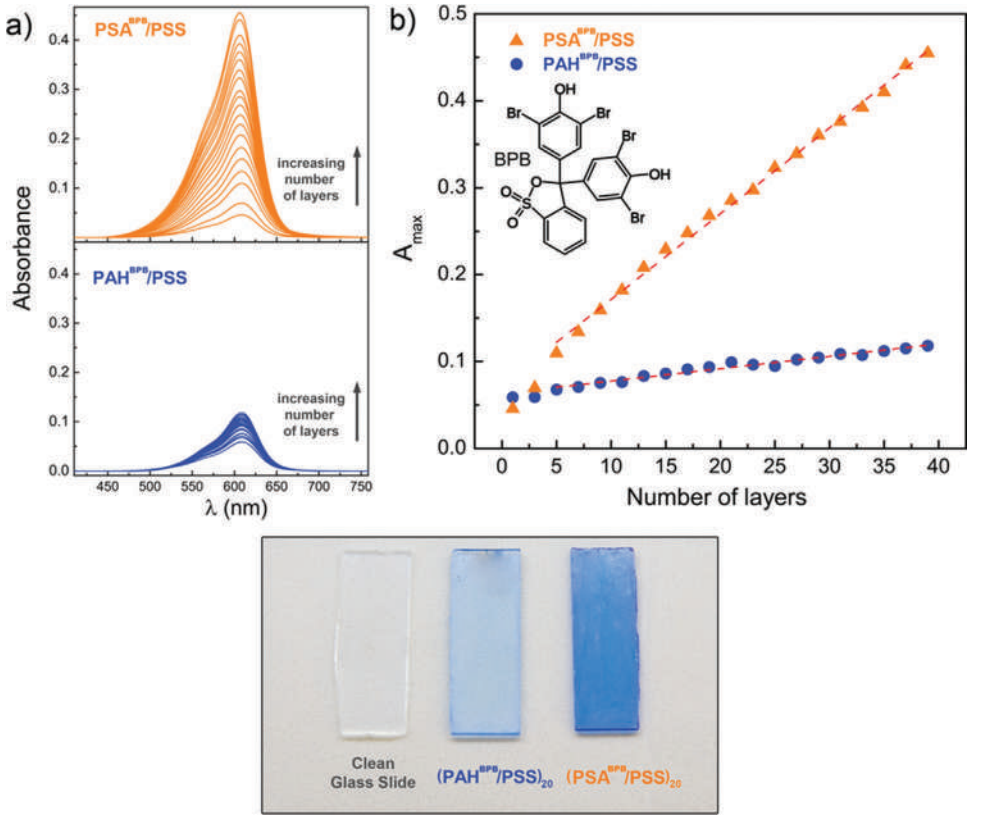

Figure 4. UV–vis measurements for the LbL assembly of BPB loaded ionically cross-linked PAH/Pi colloids (PSA^{BPB}, orange line) and BPB containing PAH aqueous solution (PAH^{BPB}, blue line) with PSS. a) Full spectra for odd layers and b) absorbance at $\lambda = 606$ nm as a function of the deposited layer number. Photographs of clean glass substrate (left panel), $(PAH^{BPB}/PSS)_{20}$ (center panel) and $(PSA^{BPB}/PSS)_{20}$ (right panel).

a result, a turbid light blue colored solution was obtained. The dye loaded PSA solution (PSA^{BPB}) was kept at room temperature for 24 h to stabilize. After this, the integrity of the particles was checked by DLS (Figure S1, Supporting Information) and no significant changes were detected respect to the initial PSA solution (Figure 1).

To evaluate the amount of BPB integrated into the PAH/Pi, the PSA^{BPB} solution was centrifugated at 10 000 rpm for 20 min and a UV–vis spectrum was performed on the supernatant. The maximum absorption in the spectrum was compared with an analogue aqueous solution constituted of a 40 µM BPB + 12 mM PAH at pH = 7.3 and found that 85% of the total BPB was successfully integrated inside the cross-linked PAH/Pi structure, only remaining 15% of the molecules in solution. This result illustrates the high loading efficiency of PSAs.

Following the aim of this work, the BPB loaded PSAs were employed as building blocks for LbL construction of thin films over glass slides. Using the methodology described on Scheme 1, the $(PSA^{BPB}/PSS)_{20}$ multilayer was built up and monitored by UV–vis spectroscopy at each deposition step. In parallel, a traditional PAH/PSS LbL was also constructed, this time by adding 40 µM of BPB into a PAH aqueous solution at pH = 7.3 (PAH^{BPB}). Figure 4a shows the UV–vis spectrum of the modified glass after modification with $(PSA^{BPB}/PSS)_n$ and $(PAH^{BPB}/PSS)_n$ as the number n of deposited layers increases. The spectra show a maximum absorption at $\lambda = 606$ nm. A red shift of 15 nm indicates that the BPB molecule interacts strongly with the amine groups of the PAH chains inside the film structure. Photographs in Figure 4 reveal that after 20 deposition cycles the glass treated with PSA^{BPB} exhibit a stronger coloration than analogous films treated with PAH^{BPB}. This result is also consistent with AFM and SPR characterizations indicating the thicker films results from the integration of PSAs.

In order to obtain the film growth rate and consequently the net BPB loading per layer, the absorption at 606 nm was plotted against the number of deposited layers (Figure 4b). A linear relation was obtained starting from the third layer of PSA^{BPB} in agreement with the SPR data showing that the adding of dye into the colloid dispersion does not affect the behavior of PSAs as building blocks in LbL deposition. From the linear regression of both PSA^{BPB}/PSS and PAH^{BPB}/PSS plots (red curves in Figure 4b), a sevenfold increase in the growth rate was obtained for the hybrid film in comparison with the traditional LbL, thus demonstrating the efficiency of the procedure and the high loading capacity. To corroborate that the film growth characteristics are directly related to the electrostatic attachment of PSAs to the underlying PSS layer, a series of control experiments were carried out comparing the absorption at 606 nm of PSA^{BPB}/PSS LbL with different pairs. Figure S3, Supporting Information shows the film construction of PSA^{BPB}/PSS, PAH^{BPB}/PSS, and two control systems: a

cationic polyelectrolyte (1 mg mL^{-1} PDDA aqueous solution) with PSA^{BPB} (PDDA/PSA^{BPB}) and 40 μM BPB aqueous solution at pH = 7.3 with PSS (BPB/PSS). Results indicated that only the PSA^{BPB}/PSS system presents both high loading capacity and a linear growth characteristic confirming that the coating is constructed from electrostatic interactions between building blocks of opposite charge.

To evaluate the amount of BPB contained in the film, a modified glass substrate was incubated in 2.5 mL of water at pH = 13. At this pH, charged ammonium groups in the PAH are deprotonated and, consequently, the interaction of the PAH chains with HPO_4^{2-} ions and PSS chains decreases and the film disintegrates completely, releasing the total content of BPB molecules. After removing the substrate, a UV–vis spectrum was performed on the solution, and the total released dye moles were obtained by means of a BPB calibration curve at pH = 13 (Figure S2, Supporting Information). For a typical 2.5 cm × 1 cm glass slide modified with $(PSA^{BPB}/PSS)_{10}$, 9 ± 2 nmols of BPB were loaded in the film, representing a total of 0.18 nmol cm^{-2} per deposited layer, assuming homogeneous distribution of material on each side of the slide.

3.4. Dye Release from the LbL Films

Having demonstrated the linear growth and the BPB loading capacity of PAH/Pi containing hybrid thin films, the controlled release of dye molecules was studied by exposing $(PSA^{BPB}/PSS)_{10}$ modified glass slides to different releasing aqueous solutions in a loop experiment until total BPB release. For quantitative analysis, after each incubation time, the substrates were removed and the BPB containing solution was analyzed by UV–vis spectroscopy.

Figure 5 shows the BPB release as a function of time for different releasing solutions. In the case of water (Figure 5a), only 40% of the total dye content was released over a month period. This could indicate that 40% of the BPB molecules inside the film structure are labile and the interaction with the cross-linked network is not too strong. The water molecules penetrate the film and solvate the BPB molecules extracting them with a slow kinetics. The remaining 60% of the BPB molecules, on the contrary, are strongly linked to the ionically cross-linked PAH/Pi structure. When the film was exposed to PBS (pH = 7.4), a 100% of the total BPB molecules were released in the month period (Figure 5b). The plot shows also that the 80% of the molecules were released in a period of 100 h (about 4 days). This result indicates that an increase in the ionic strength allows the molecules to transfer into the solution phase more easily. Possibly, the salt and phosphate anions present in high concentrations in the PBS solution can diffuse into the film and break some ion pairs within the ionic network, destabilizing the matrix and facilitating the diffusion of the dye molecules. Also, the faster BPB release into PBS media could have been caused by the salt-induced desorption of the ionically bonded BPB from PAH. Previously, Lapitsky and coworkers observed this reduction in cross-link density induced by salt effects in gel-like coacervates prepared from the ionic self-assembly of PAH with either pyrophosphate or tripolyphosphate.[51,63] On the other hand, these gels showed a high capacity to encapsulate small molecules and release them over multiple-month timescales.[64–67] The slow release rate is possibly due to a higher cross-link density generated by the use of ionic cross-linkers with higher net charge as compared to single phosphate. This increased cross-linking generates a more efficient diffusion barrier for the encapsulated molecules. In our system, the release rate may be modulated by varying the cross-link density using different amounts of Pi in the PSAs preparation process. Further investigation must be carried out in order to determine the effect of the amount of cross-linking and the swelling degree of the film in contact with water and PBS to fully understand the mechanism of dye release.

Subsequently, the effect of the pH change on the release kinetics was analyzed. Knowing that the PAH/Pi structure is mainly stabilized by the electrostatic interaction between the charged amine groups of the PAH and the HPO_4^{2-} ions, a shift in the solution pH should have a direct impact on the release kinetics and, eventually, the film total disintegration.[40] At acidic pH, the protonation of HPO_4^{2-} ions affects the film integrity by weakening the ionic cross-linking of the supramolecular structure. On the other hand, at alkaline pH values, the deprotonation of the amine groups is the responsible of the film instability.[58,59] In this way, the modified substrates were incubated in PBS solution at different pH values, such as pH = 5 (Figure 4c), pH = 8 (Figure 4d), pH = 10.5 (Figure 4e), and pH = 2 (Figure 4f). For slightly acidic and basic pH (5 and 8), 80% of the dye molecules were released in a period of 24 h and the total amount of loaded BPB was released after 15 days of treatment. These experiments show that the variation of the external pH weakens the PAH/Pi interactions leading to an increase in the kinetics of film disintegration and, consequently, in the rate of dye transfer to the solution phase. When the pH was adjusted at extreme values, that is, 10.5 and 2, the BPB transfer to the solution was even more effective, achieving 80% of release after 18 and 1 h respectively. The total amount of dye content was released in 10 days for PBS at pH = 10.5 and 8 h for PBS at pH = 2. Furthermore, if the pH is increased above 11, the film is removed completely after a few seconds by total deprotonation of the amine groups.

These results demonstrate that PSAs formed by direct interaction between PAH and Pi anions can be self-assembled with PSS and incorporate/release BPB into/from films.

4. Conclusions

In this work, we presented the construction of hybrid thin films constituted of two different materials: a supramolecular network of ionically cross-linked PAH chains with Pi as a positively charged building block (PSA) and PSS as a negatively charged counterpart. The film preparation was carried out by employing the LbL technique with alternated deposition of each material. The PSA colloids were prepared by a mild and one-pot synthesis exhibiting a remarkable stability in solution after a post-synthesis pH adjustment. The long-term stability of the colloidal dispersion resulted to be crucial in order to obtain a linear film growing as a function of the number of deposited layers. SPR, AFM, and UV–vis spectroscopy experiments

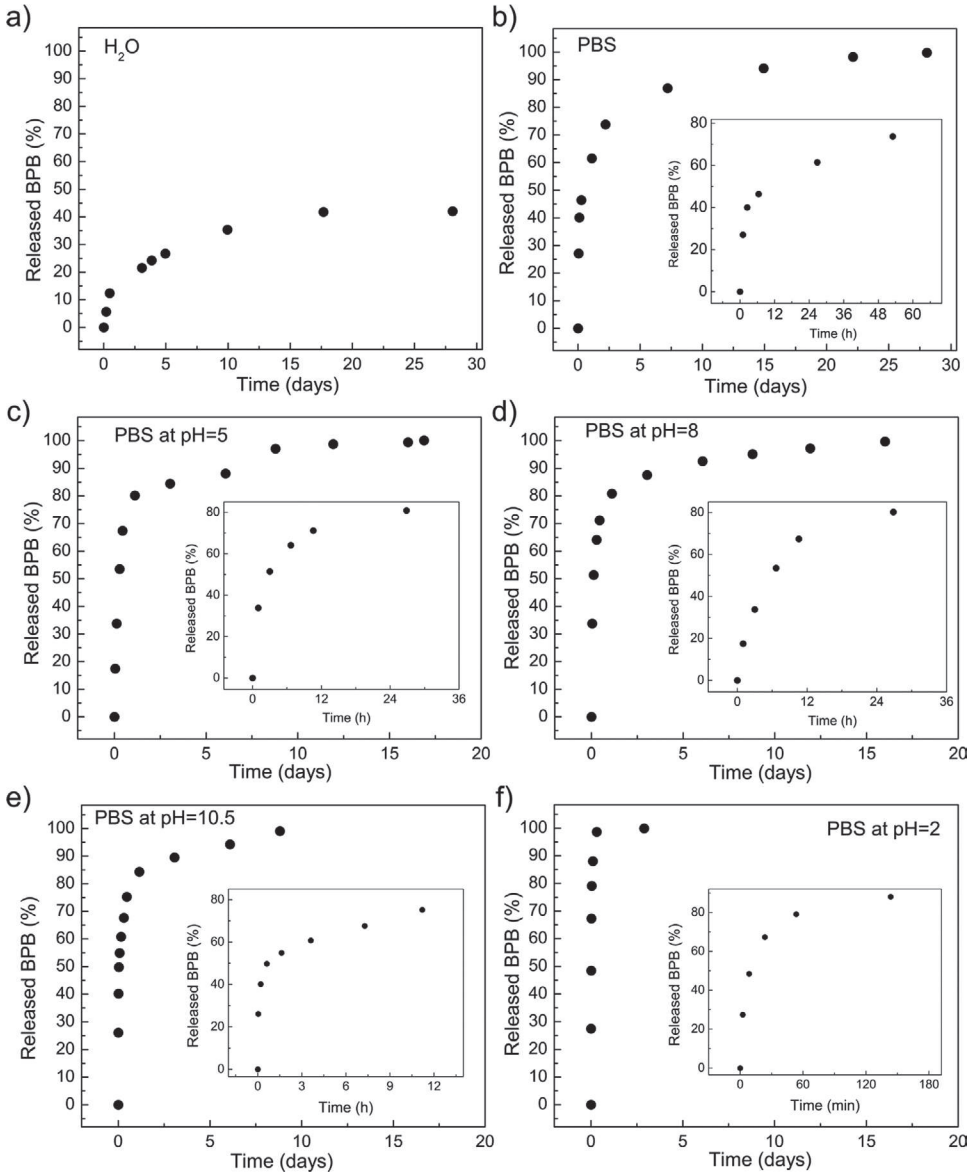

Figure 5. Controlled releasing of bromophenol blue (BPB) from $(PSA^{BPB}/PSS)_{10}$ modified glass slides. Plots of released percentage as function of time for different releasing solutions: a) Water, b) PBS, and c) PBS at pH = 5, d) pH = 8, e) pH = 10.5, and f) pH = 2.

showed that the growth rate of hybrid film PSA/PSS is 5–8 times higher than that corresponding to traditional (PAH/PSS) LbL films assembled under the same experimental conditions.

By exploiting the functional capabilities of these films, a negatively charged dye molecule BPB was incorporated in the film by electrostatic integration in PSAs, followed by LbL assembly with PSS. The loading performance was monitored by UV–vis spectroscopy and a linear relation was obtained between the number of deposited layers and the film absorbance. Finally, hybrid films assembled on glass slides were exposed to different aqueous solutions to evaluate the release of BPB as a function of time. Results indicated that it is possible to achieve a controlled release in PBS solution by easily modulating the release rates through pH changes. In this way, it has been possible to vary the release times between minutes and months.

We believe that this new nanoarchitectonic approach can be used to create hybrid thin films with remarkable properties for loading and release of therapeutic model drugs in physiological conditions. Further investigation must be carried out in order to modulate the film growth rate and the loading of molecules per layer by variations of PSA synthesis conditions.

Supporting Information

Supporting Information is available from the Wiley Online Library or from the author.

Acknowledgements

S.E.H. and M.L.A. contributed equally to this work. This work was supported by CONICET, ANPCyT (PICT 2013-0905, PICT 2016-1680), the Austrian Institute of Technology GmbH (AIT-CONICET Partner Group, Exp. 4947/11, Res. No. 3911, 28-12-2011), Universidad Nacional de La Plata (UNLP), S.E.H. and M.L.A. acknowledge CONICET for their postdoctoral fellowships. M.L.C., C.v.B, W.A.M., and O.A. are staff members of CONICET.

Conflict of Interest

The authors declare no conflict of interest.

Keywords

controlled release, hybrid films, layer-by-layer assembly, loading capacity, supramolecular colloids

Received: March 7, 2019
Revised: April 22, 2019
Published online:

[1] G. Decher, in *Multilayer Thin Film*. Wiley-VCH, Weinheim, Germany **2002**, pp. 1–46.
[2] K. Ariga, J. P. Hill, Q. Ji, *Phys. Chem. Chem. Phys.* **2007**, *9*, 2319.
[3] K. Ariga, Q. Ji, J. P. Hill, Y. Bando, M. Aono, *NPG Asia Mater.* **2012**, *4*, e17.
[4] X. Zhang, Y. Xu, X. Zhang, H. Wu, J. Shen, R. Chen, Y. Xiong, J. Li, S. Guo, *Prog. Polym. Sci.* **2019**, *89*, 76.
[5] G. Decher, *Science* **1997**, *277*, 1232.
[6] F. Caruso, H. Möhwald, *J. Am. Chem. Soc.* **1999**, *121*, 6039.
[7] D. Pallarola, C. von Bildering, L. I. Pietrasanta, N. Queralto, W. Knoll, F. Battaglini, O. Azzaroni, *Phys. Chem. Chem. Phys.* **2012**, *14*, 11027.
[8] R. A. Caruso, A. Susha, F. Caruso, *Chem. Mater.* **2001**, *13*, 400.
[9] F. Caruso, M. Spasova, V. Salgueiriño-Maceira, L. M. Liz-Marzán, *Adv. Mater.* **2001**, *13*, 1090.
[10] A. J. Khopade, F. Caruso, *Nano Lett.* **2002**, *2*, 415.
[11] M. L. Cortez, A. Lorenzo, W. A. Marmisollé, C. Von Bilderling, E. Maza, L. Pietrasanta, F. Battaglini, M. Ceolín, O. Azzaroni, *Soft Matter* **2018**, *14*, 1939.
[12] M. Ali, B. Yameen, J. Cervera, P. Ramírez, R. Neumann, W. Ensinger, W. Knoll, O. Azzaroni, *J. Am. Chem. Soc.* **2010**, *132*, 8338.
[13] G. E. Fenoy, E. Maza, E. Zelaya, W. A. Marmisollé, O. Azzaroni, *Appl. Surf. Sci.* **2017**, *416*, 24.
[14] J. Hiller, J. D. Mendelsohn, M. F. Rubner, *Nat. Mater.* **2002**, *1*, 59.
[15] A. M. Balachandra, J. Dai, M. L. Bruening, *Macromolecules* **2002**, *35*, 3171.
[16] N. Jessel, F. Atalar, P. Lavalle, J. Mutterer, G. Decher, P. Schaaf, J.-C. Voegel, J. Ogier, *Adv. Mater.* **2003**, *15*, 692.
[17] E. Vázquez, D. M. Dewitt, P. T. Hammond, D. M. Lynn, *J. Am. Chem. Soc.* **2002**, *124*, 13992.
[18] R. M. Flessner, Y. Yu, D. M. Lynn, *Chem. Commun.* **2011**, *47*, 550.
[19] X. Zhang, X. Zhang, S. Guo, *Polym. Eng. Sci.* **2019**, *59*, E348.
[20] S. Pavlukhina, S. Sukhishvili, *Adv. Drug Delivery Rev.* **2011**, *63*, 822.
[21] S. Park, U. Han, D. Choi, J. Hong, *Biomater. Res.* **2018**, *22*, 29.
[22] E. Kharlampieva, I. Erel-Unal, S. A. Sukhishvili, *Langmuir* **2007**, *23*, 175.
[23] V. A. Kozlovskaya, E. P. Kharlampieva, I. Erel-Unal, S. A. Sukhishvili, *Polym. Sci. Ser. A* **2009**, *51*, 719.
[24] L. Zhang, J. Sun, *Chem. Commun.* **2009**, *0*, 3901.
[25] K. Katagiri, R. Hamasaki, K. Ariga, J. Kikuchi, *J. Am. Chem. Soc.* **2002**, *124*, 7892.
[26] M. Michel, A. Izquierdo, G. Decher, J.-C. Voegel, P. Schaaf, V. Ball, *Langmuir* **2005**, *21*, 7854.
[27] M. Coustet, J. Irigoyen, T. A. Garcia, R. A. Murray, G. Romero, M. S. Cortizo, W. Knoll, O. Azzaroni, S. E. Moya, *J. Colloid Interface Sci.* **2014**, *421*, 132.
[28] Z. Zhu, S. A. Sukhishvili, *J. Mater. Chem.* **2012**, *22*, 7667.
[29] M. J. Serpe, C. D. Jones, L. A. Lyon, *Langmuir* **2003**, *19*, 8759.
[30] M. J. Serpe, K. A. Yarmey, C. M. Nolan, L. A. Lyon, *Biomacromolecules* **2005**, *6*, 408.
[31] K. C. Clarke, L. A. Lyon, *Langmuir* **2013**, *29*, 12852.
[32] C. M. Nolan, M. J. Serpe, L. A. Lyon, *Biomacromolecules* **2004**, *5*, 1940.
[33] L. A. Lyon, Z. Meng, N. Singh, C. D. Sorrell, A. St. John, *Chem. Soc. Rev.* **2009**, *38*, 865.
[34] J. C. Gaulding, M. H. Smith, J. S. Hyatt, A. Fernandez-Nieves, L. A. Lyon, *Macromolecules* **2012**, *45*, 39.
[35] E. Maza, C. Von Bilderling, M. L. Cortez, G. Díaz, M. Bianchi, L. I. Pietrasanta, J. M. Giussi, O. Azzaroni, *Langmuir* **2018**, *34*, 3711.
[36] L. Wang, X. Wang, M. Xu, D. Chen, J. Sun, *Langmuir* **2008**, *24*, 1902.
[37] Y. Lapitsky, *Curr. Opin. Colloid Interface Sci.* **2014**, *19*, 122.
[38] V. S. Murthy, R. K. Rana, M. S. Wong, *J. Phys. Chem. B* **2006**, *110*, 25619.
[39] H. G. Bagaria, M. S. Wong, *J. Mater. Chem.* **2011**, *21*, 9454.
[40] W. A. Marmisollé, J. Irigoyen, D. Gregurec, S. Moya, O. Azzaroni, *Adv. Funct. Mater.* **2015**, *25*, 4144.
[41] M. L. Agazzi, S. E. Herrera, M. L. Cortez, W. A. Marmisollé, C. von Bilderling, L. I. Pietrasanta, O. Azzaroni, *Soft Matter* **2019**, *15*, 1640.
[42] M. Sumper, S. Lorenz, E. Brunner, *Angew. Chem., Int. Ed.* **2003**, *42*, 5192.
[43] E. Brunner, K. Lutz, M. Sumper, *Phys. Chem. Chem. Phys.* **2004**, *6*, 854.
[44] K. Lutz, C. Gröger, M. Sumper, E. Brunner, *Phys. Chem. Chem. Phys.* **2005**, *7*, 2812.
[45] L. D'Agostino, M. Di Pietro, A. Di Luccia, *FEBS J.* **2005**, *272*, 3777.
[46] M. Mouslmani, J. M. Rosenholm, N. Prabhakar, M. Peurla, E. Baydoun, D. Patra, *RSC Adv.* **2015**, *5*, 18740.
[47] J. Yu, M. A. Yaseen, B. Anvari, M. S. Wong, *Chem. Mater.* **2007**, *19*, 1277.
[48] P. Andreozzi, E. Diamanti, K. R. Py-Daniel, P. R. Cáceres-Vélez, C. Martinelli, N. Politakos, A. Escobar, M. Muzi-Falconi, R. Azevedo, S. E. Moya, *ACS Appl. Mater. Interfaces* **2017**, *9*, 38242.
[49] F. Z. Henari, A. Al-Saie, K. G. Culligan, *J. Nonlinear Opt. Phys. Mater.* **2012**, *21*, 1250015.
[50] S. E. Herrera, M. L. Agazzi, M. L. Cortez, W. A. Marmisollé, M. Tagliazucchi, O. Azzaroni, *Chem. Phys. Chem.* **2019**, *20*, 1044.
[51] P. G. Lawrence, Y. Lapitsky, *Langmuir* **2015**, *31*, 1564.
[52] K. E. Tettey, J. W. C. Ho, D. Lee, *J. Phys. Chem. C* **2011**, *115*, 6297.
[53] G. Agrawal, R. Agrawal, *Polymers* **2018**, *10*, 418.
[54] S. Schmidt, H. Motschmann, T. Hellweg, R. von Klitzing, *Polymer* **2008**, *49*, 749.
[55] R. Contreras-Cáceres, J. Pacifico, I. Pastoriza-Santos, J. Pérez-Juste, A. Fernández-Barbero, L. M. Liz-Marzán, *Adv. Funct. Mater.* **2009**, *19*, 3070.
[56] S. Wellert, Y. Hertle, M. Richter, M. Medebach, D. Magerl, W. Wang, B. Demé, A. Radulescu, P. Müller-Buschbaum, T. Hellweg, R. von Klitzing, *Langmuir* **2014**, *30*, 7168.
[57] A. Mourran, Y. Wu, R. A. Gumerov, A. A. Rudov, I. I. Potemkin, A. Pich, M. Möller, *Langmuir* **2016**, *32*, 723.
[58] K. D. Kelly, J. B. Schlenoff, *ACS Appl. Mater. Interfaces* **2015**, *7*, 13980.

[59] L. Wang, D. Chen, J. Sun, *Langmuir* **2009**, *25*, 7990.
[60] X. Wang, L. Zhang, L. Wang, J. Sun, J. Shen, *Langmuir* **2010**, *26*, 8187.
[61] J. Zhang, D. Chen, Y. Li, J. Sun, *Polymer* **2013**, *54*, 4220.
[62] J. Courbat, D. Briand, J. Damon-Lacoste, J. Wöllenstein, N. F. de Rooij, *Sens. Actuators, B.* **2009**, *143*, 62.
[63] Y. Huang, P. G. Lawrence, Y. Lapitsky, *Langmuir* **2014**, *30*, 7771.
[64] P. G. Lawrence, P. S. Patil, N. D. Leipzig, Y. Lapitsky, *ACS Appl. Mater. Interfaces* **2016**, *8*, 4323.
[65] U. K. De Silva, J. L. Brown, Y. Lapitsky, *RSC Adv.* **2018**, *8*, 19409.
[66] X. Z. Shu, K. J. Zhu, *Eur. J. Pharm. Biopharm.* **2002**, *54*, 235.
[67] S. R. Bhatia, S. F. Khattak, S. C. Roberts, *Curr. Opin. Colloid Interface Sci.* **2005**, *10*, 45.